

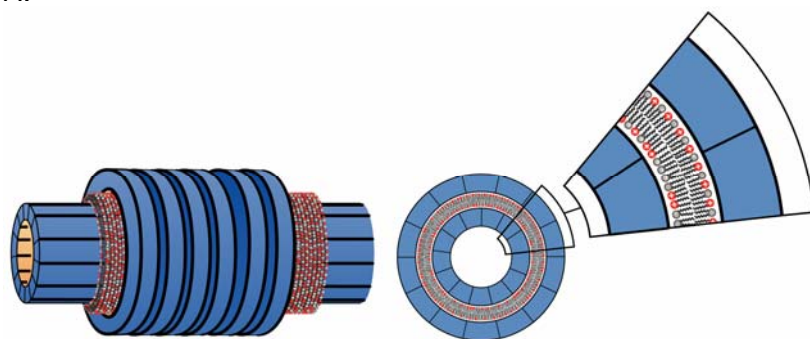
Cationic Liposome-Microtubule Complexes: Lipid-Protein Bio-Nanotubes with Open or Closed Ends

Uri Raviv^{*,†}, Daniel J. Needleman^{*,†}, Youli Li^{*,†}, Herbert P. Miller[†], Leslie Wilson[†], and Cyrus R. Safinya^{*,†}

* Materials Department, Physics Department † Molecular, Cellular, and Developmental Biology Department, Biomolecular Science and Engineering Program, University of California, Santa Barbara, CA 93106

In this work we explored the structures that form when cationic liposomes are mixed with microtubules (MTs). Using synchrotron small angle X-ray diffraction (SAXRD) and transmission electron microscopy (TEM), we find two novel structures(1). For soft and intermediate rigid membranes we find that the cationic liposomes spread and coat the MTs and the external lipid layer is decorated by tubulin oligomers, forming a novel lipid-protein nanotube (LPN). By controlling the cationic lipid/tubulin stoichiometry, $R_{CL/T}$, of the complex the LPN can switch between a state with open ends (Sketch 1A) to a state with closed ends with lipid caps (Sketch 1B). This forms the basis for controlled drug encapsulation and release.

A.



B.



Sketch 1. A. Lipid protein nanotube (LPN) with open ends and a cross section. B. LPN with closed end and lipid caps.

For low membrane charge density, we find that vesicles adsorb onto the MT and appear as 'beads on a rod' (BOR). This is the most trivial structure that can form when vesicles interact with polyelectrolytes and was previously hypothesized for cationic lipid-DNA complexes(2), but later was experimentally(3, 4) proven unstable. Here we discovered for the first time how to obtain BOR. This state however seems to be, a kinetically trapped state. The ground state of the system follows the MT template and forms the LPN.

MTs are net negatively charged polymers, which self-assemble from tubulin protein subunits into hollow cylinders, which are ~26 nm in diameter. The tubulin dimers are arranged head to tail in protofilaments and form the MT wall.

Tubulin was purified from bovine brains and was polymerized and taxol stabilized as described (1, 5). The cationic lipid used was dioleoyl($C_{18:1}$)- trimethyl ammonium propane (DOTAP). The membrane charge density, σ , was adjusted by adding a homologous neutral lipid of the same hydrophobic tail to the charged lipid, but with the phosphatidylcholine (PC) head group instead (DOPC). Equal volumes of MTs and liposome solutions were mixed and the resulting complexes were characterized by transmission electron microscopy (TEM) and small angle X-ray diffraction (SAXRD) performed at Stanford Synchrotron Radiation Laboratory, beam-line 4-2.

The mole fraction of cationic lipids in the membrane is given by

$$x_{CL} \equiv N_{CL}/(N_{CL}+N_{NL}),$$

where N_{CL} and N_{NL} are the numbers of cationic and neutral lipids, respectively. The relative cationic lipid/tubulin stoichiometry, $R_{CL/T}$, is defined as

$$R_{CL/T} \equiv N_{CL}/N_T,$$

where N_T is the number of tubulin dimers. $R_{CL/T} \approx 40$ is the mixing isoelectric point.

A set of TEM images covering the structures in the phase diagram of MT-membrane complexes are shown in Figure 1. For cationic lipid mole fraction, $x_{CL} = 0.1$, we initially find the weakly positive charged vesicles ('beads') adsorbed onto the negatively charged microtubule, MT, wall ('rod'), forming the beads on a rod, BOR (Figure 1, lower right). Bridges are occasionally formed between adjacent MTs forming small sized bundles of MTs cross-linked via vesicles (Figure 1, lower center). This state is, however, kinetically trapped: over longer times, ~ 60 hrs, the adsorbed vesicles "wet" the MT surface, forming the lipid-protein nanotube, LPN (Figure 1, lower left). For $x_{CL} > 0.1$ the LPN forms immediately upon mixing. The images reveal that the LPN is made of three layers: Intact MTs are coated by a lipid bilayer (appears brighter in the images, as the ionic stain avoids the hydrophobic lipid tails), which in turn are coated by tubulin oligomers forming rings or spirals. The oligomer orientation is perpendicular to the internal MT protofilament direction and their density increases with x_{CL} . The three layered LPN structure arises because of the mismatch between the charge densities of MTs and cationic membranes. The oligomers coat the external lipid monolayer to optimize the electrostatic interactions and counterion release.

At a given mole fraction of cationic lipids, x_{CL} , when the total MT surface area exceeds the total membrane area, the MTs are only partially coated (Figure 1, $x_{CL} = 0.5$ and cationic lipid/tubulin stoichiometry, $R_{CL/T} = 40$), forming LPN with open ends. When the reverse is true, some of the excess vesicles are attached primarily to the ends of the LPNs (Figure 1, $x_{CL} = 0.5$, $R_{CL/T} = 120$), forming LPN with closed ends with lipid caps. The oligomer density at a given x_{CL} is similar for both open and closed LPNs. The ability to switch from open to closed LPNs forms the basis of controlled drug encapsulation and release.

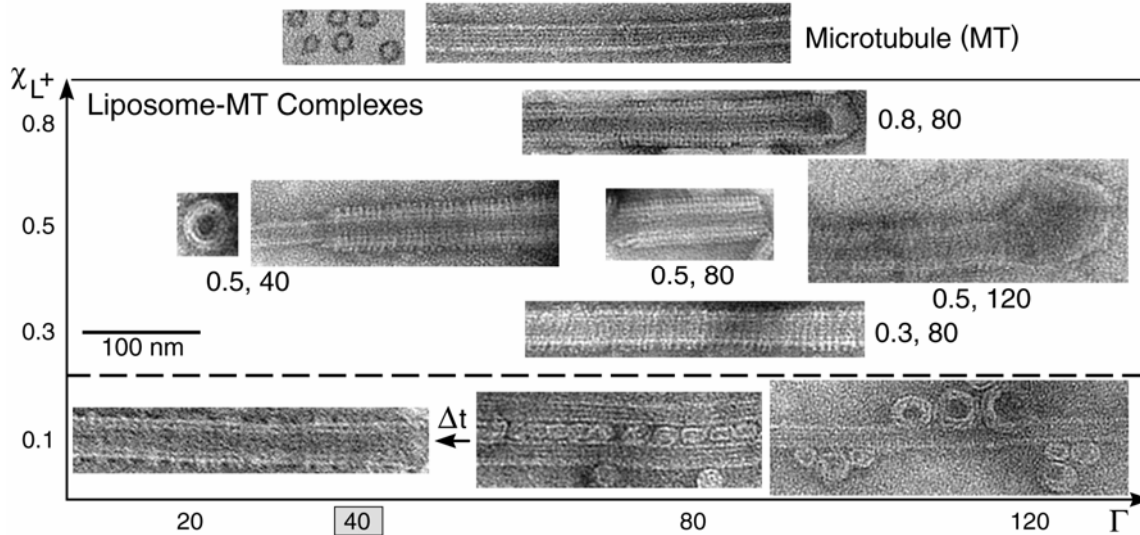


Figure 1. *Transmission electron microscopy images of the various states.* Whole mount images of pure MTs (top, right), as a control, and liposomes-MT complexes, using DOTAP/DOPC solutions with $x_{CL} \equiv N_{CL}/(N_{CL}+N_{NL})$ and $R_{CL/T} \equiv N_{CL}/N_T$ values as indicated. For $x_{CL} = 0.1$ (below the broken line) the kinetically trapped BOR and bridging states are shown on the right and the LPN state after time $\Delta t \sim 60$ hrs, (indicated by arrow) is shown on the left. Cross sections of pure MT (top, left) and the LPN structure (little square) are also shown. The mixing isoelectric point $R_{CL/T} = 40$ is marked.

TEM images and SAXRD measurements performed on pure microtubule, MT, solutions (Figures 1 and 2) and are in agreement with earlier studies(5-9). The SAXRD profile of MTs (Figure 2A) is consistent with the form factor of isotropic hollow cylinders (Figure 2B). Based on MT structural data (6, 10), we modeled the MT as three concentric cylindrical shells, of a high electron density region surrounded by two low ones, as shown in Figure 2C, keeping the total wall thickness and mean electron density as those of MTs. The thickness and location of the high electron density region, within the MT wall, and the inner MT radius are fitting parameters in this model.

A set of SAXRD data for MT-lipid (DOTAP/DOPC) complexes is shown in Figure 2A. For $x_{CL} > 0.1$ the SAXRD scans show broad oscillations that are different from that of MTs and correspond to the form factor of the LPNs. For $x_{CL} = 0.1$, 2 hrs after MTs and membranes were mixed, the SAXRD scan is consistent (for $q > 0.2 \text{ nm}^{-1}$) with the form factor of isotropic MT solutions. At smaller angles there is an additional broad Gaussian correlation peak, centered at $q = 0.139 \text{ nm}^{-1}$, corresponding to 45 nm. The SAXRD scan is therefore consistent with the BOR and bridging states (Figure 1). The existence of a correlation peak suggests that the size distribution of the bridging vesicles is relatively narrow. SAXRD scans taken 60 hrs after mixing (Figure 2A), show that this structure slowly evolves into the form factor of the LPNs.

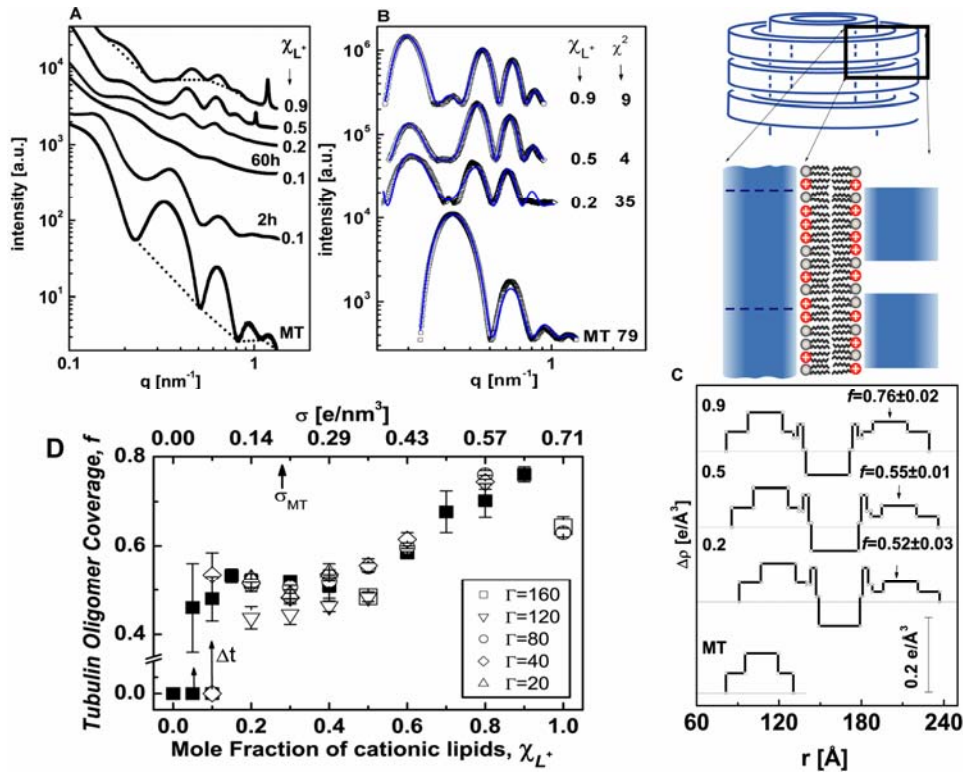


Figure 2. *Synchrotron small angle x-ray scattering data, analysis and a state diagram.* **A.** Radially averaged scattering intensities of MTs and MT-lipid complexes (solid symbols), using DOTAP/DOPC solutions with $\chi_{CL} \equiv N_{CL}/(N_{CL}+N_{NL})$ as indicated in the figure. $R_{CL/T} \equiv N_{CL}/N_T$ is given by $R_{CL/T} = 160 \cdot \chi_{CL}$, corresponding to the point at which the total amount of lipid is exactly enough to coat each MT with a bilayer. For $\chi_{CL} = 0.1$ two scans are shown, 2 hrs and 60 hrs after preparing the sample. The broken curves are examples of the assumed background(5, 7, 8). **B.** Scattering data from **A**, following background subtraction (open symbols). The solid curves are the fitted scattering models. Their χ^2 values are as in the figure. **C.** The variation of the radial electron density, $\Delta\rho(r)$, relative to water (broken lines), of the MTs and complex walls, obtained from fitting the scattering data in **B** to models of concentric cylinders. r is the distance from the center of the cylinders. The tubulin oligomer coverage, f , values obtained from the nonlinear fit are indicated on the right side. The schematic represents a vertical cut through the MT-membrane-tubulin complex wall, corresponding to $\Delta\rho(r)$. **D.** State diagram: f as a function of χ_{CL} or the membrane charge density, σ , when lipids can fully cover the MTs. Each data point is based on scattering data and models as in **A-C**. Solid squares corresponds to $R_{CL/T} = 160 \cdot \chi_{CL}$. Open symbols represent different $R_{CL/T}$ values, as indicated in the Figure. For $0 < \chi_{CL} \leq 0.1$ we initially get $f = 0$ (corresponding to the BOR structure), over time, $\Delta t \sim 60$ hrs, shown by the arrows, we obtain LPNs with higher f values.

To gain quantitative insight into the organization of the complexes, we analyze the background subtracted SAXRD data, shown in Figure 2B, by fitting to a model. To model the data, a series of power laws that pass through the minima of the scattering intensities was subtracted. We extend the isotropic concentric cylindrical shells model of MTs to include the second lipid bilayer and the third tubulin layer (Figure 2C). The radial electron density profile of the inner MT wall and outer tubulin monolayer are based on the fit to the MT scattering data. The parameters for the electron density profile of the lipid bilayer are based on literature data(11, 12). Finally, the third tubulin layer is multiplied by the fraction, f , of tubulin coverage relative to the inner MT wall. f is the unknown parameter in this model and is allowed to float freely. The scattering models (Figure 2B) fit very well to the data.

The SAXRD scans may also have a resolution limited strong peak (Figure 2A $x_{CL} = 0.5, 0.9$), corresponding to excess lipid vesicles in the lamellar phase that are associated with the complexes (closing the ends of the LPNs, see Figure 1).

Figure 2D summarizes a series of SAXRD scans as in Figure 2A, analyzed as in Figure 2B&C. A states diagram is obtained, in which f is plotted as a function of x_{CL} or the membrane charge density, σ , at various $R_{CL/T}$ values. For $x_{CL} = 0$, corresponding to pure DOPC membrane, SAXRD scans show only the isotropic MT form factor. This state (indicated as $f = 0$) is stable for days, indicating that the LPN is induced by the cationic lipids. At $0 < x_{CL} \leq 0.1$, we have kinetically trapped states of BOR and bridging (also indicated by $f=0$) that evolve slowly into the LPN. For $x_{CL} > 0.1$, we only see the LPN with f values that increase monotonically with x_{CL} . $R_{CL/T}$ has little effect on f , in agreement with the TEM images (Figure 1).

We have described and characterized the beads on a rod and the lipid-protein nanotube, LPN, structures, the conditions for their formation and the transition between them. By controlling the cationic lipid /tubulin stoichiometry the LPN can be tailored to have open or closed ends with lipid caps. Because the main governing concepts for this self assembly are general(13, 14) we expect synthetic analogs to follow similar assembly pathways, so that synthetic versions mimicking the LPNs (e.g. replacing microtubules with rigid polyelectrolytes) may have applications in chemical encapsulation and delivery. Finally, positively charged membranes are commonly used for non-viral drug and gene delivery and introduced into cells(4). Our results suggest that their association with microtubules, leading to possible changes in their structure and dynamics in cells, is an important consideration in delivery applications using cationic lipids.

Acknowledgements

The work was performed using state-of-the-art synchrotron x-ray scattering techniques at the Stanford Synchrotron Radiation Laboratory (SSRL) at beam-line 4-2, combined with sophisticated electron microscopy at the University of California, Santa Barbara. This project is supported by NSF DMR- 0503347, CTS-0404444, and NIH GM-59288 and NS-13560. The Stanford Synchrotron radiation laboratory is supported by the U.S. DOE. U.R. acknowledges the support of the International Human Frontier Science Program Organization and the European Molecular Biology Organization.

Primary Citation

Raviv, U., Needleman, D. J., Li, Y., Miller, H. P., Wilson, L. & Safinya, C. R. (2005) *Proc. Natl. Acad. Sci. USA* **102**, 11167-11172.

References

1. Raviv, U., Needleman, D. J., Li, Y., Miller, H. P., Wilson, L. & Safinya, C. R. (2005) *Proc. Natl. Acad. Sci. USA* **102**, 11167-11172.
2. Felgner, P. L., Gadek, T. R., Holm, M., Roman, R., Chan, H. W., Wenz, M., Northrop, J. P., Ringold, G. M. & Danielsen, M. (1987) *Proc. Natl. Acad. Sci. USA* **84**, 7413-7417.
3. Radler, J. O., Koltover, I., Salditt, T. & Safinya, C. R. (1997) *Science* **275**, 810-814.
4. Koltover, I., Salditt, T., Radler, J. O. & Safinya, C. R. (1998) *Science* **281**, 78-81.
5. Needleman, D. J., Ojeda-Lopez, M. A., Raviv, U., Miller, H. P., Wilson, L. & Safinya, C. R. (2004) *Proc. Natl. Acad. Sci. USA* **101**, 16099-16103.

6. Li, H., DeRosier, D. J., Nickolson, W. V., Nogales, E. & Downing, K. H. (2002) *Structure* **10**, 1317-1328.
7. Andreu, J. M., Bordas, J., Diaz, J. F., Garcia de Ancos, J., Gil, R., Medrano, F. J., Nogales, E., Pantos, E. & Towns-Andrews, E. (1992) *J. Mol. Biol.* **226**, 169-184.
8. Fernando-Diaz, J., Andreu, J. M., Diakun, G., Towns-Andrews, E. & Bordas, J. (1996) *Biophys. J.* **70**, 2408-2420.
9. Needleman, D. J., Ojeda-Lopez, M. A., Raviv, U., Ewert, K., Jones, J. B., Miller, H. P., Wilson, L. & Safinya, C. R. (2004) *Phys. Rev. Lett.* **93**, 198104-1.
10. Lee, J. C., Frigon, R. P. & Timasheff, S. N. (1973) *J. Biol. Chem.* **248**, 7253-7262.
11. Liu, Y. F. & Nagle, J. F. (2004) *Phys. Rev. E* **69**, Art. No. 040901.
12. Wong, G. C. L., Tang, J. X., Lin, A., Li, Y., Janmey, P. A. & Safinya, C. R. (2000) *Science* **288**, 2035-2039.
13. May, S. & Ben-Shaul, A. (1997) *Biophys. J.* **73**, 2427-2440.
14. Harries, D., Ben-Shaul, A. & Szleifer, I. (2004) *J. Phys. Chem. B* **108**, 1491-1496.

SSRL is supported by the Department of Energy, Office of Basic Energy Sciences. The SSRL Structural Molecular Biology Program is supported by the Department of Energy, Office of Biological and Environmental Research, and by the National Institutes of Health, National Center for Research Resources, Biomedical Technology Program, and the National Institute of General Medical Sciences.